Aligned poly-L-Lactic Acid (PLLA) nanofibres induce self-assembly of primary cortical neurons into 3D cell clusters

Weir, N.*, Stevens, R., Wagner, S., Miles, A.K., Ball, G.R., Howard, C., Chemmarappally, J.M., McGinnity, T.M., Hargreaves, A.J., Tinsley, C. J.

School of Science and Technology, Nottingham Trent University, Clifton Lane, Nottingham, NG11 8NS

*Corresponding author:

Nicholas Weir

Nick.J.Weir92@gmail.com

Number of words: 3,433

Keywords: PLLA, Nanofibres, Neuronal Architecture, 3D Cell Culture

Acknowledgements: This work was supported by a Nottingham Trent University studentship awarded to Nicholas Weir

Abstract

Relative to two-dimensional (2D) culture, three-dimensional (3D) culture of primary neurons has yielded increasingly physiological responses from cells. Electrospun nanofibre scaffolds are frequently used as a 3D biomaterial support for primary neurons in neural tissue engineering whilst hydrophobic surfaces typically induce aggregation of cells. Poly-L-lactic acid (PLLA) was electrospun as aligned PLLA nanofibre scaffolds to generate a structure with both qualities. Primary cortical neurons from E18 Sprague Dawley rats cultured on aligned PLLA nanofibres generated 3D clusters of cells that extended highly aligned, fasciculated neurite bundles within 10 days. These clusters were viable for 28 days and responsive to AMPA and GABA. Relative to the 2D culture, the 3D cultures exhibited a more developed profile; mass spectrometry demonstrated an upregulation of proteins involved in cortical lamination, polarisation, axon fasciculation and a downregulation of immature neuronal markers. Use of artificial neural network inference suggests that the increased formation of synapses may drive the increase development that is observed for the 3D cell clusters. This research suggests that aligned PLLA nanofibres may be highly useful for generating advanced 3D cell cultures for high throughput systems.

Abbreviations

ANNI; artificial neural network inference

DAPI; 4',6-diamidino-2-phenylindole

DIV; days *in vitro*

ECM; extracellular matrix

HFIP; hexafluoroisopropanol

LDH; lactate dehydrogenase

ND; narrow diameter

PBS; phosphate buffered saline

PLLA; poly-L-lactic acid

P-PLLA; plasma treated PLLA

SEM; scanning electron microscope

1. Introduction

Dissociated neurons in two-dimensional (2D) cell culture have been utilised as an *in vitro* model of the central nervous system; however, cells grown in 3D culture demonstrate more appropriate physiological behaviours than their 2D counterparts. Gene expression, cell signalling, morphology, migration, proliferation and susceptibility to pathologies are documented to be more physiological in 3D culture environments[1]. This in part may be due to the different mechanical environments that cells are exposed to in the efforts to generate these 3D cultures. Mechanical properties such as elastic modulus[2-4], conductivity[5,6] and wettability[7] have all been demonstrated to influence cellular behaviours and thus, material properties likely influence the increased physiological responses that cells exhibit.

Due to the greater physiological relevance of 3D culture relative to conventional 2D cell culture, they are used for a diverse range of research purposes[8,9]. Cerebral cortical organoids are the gold standard for 3D cell culture and recapitulate various physiological and structural properties of the brain[10,11]. However, whilst organoids are physiologically representative of the cerebral cortex, they are limited with regards to use in high-throughput methodologies due to the time taken to generate them and the number of steps required by the protocol. An ability to rapidly produce simple, 3D neuronal architectures, such as those resembling white (i.e. aligned axons or neurites) and grey matter (i.e. grouped neuronal cell bodies), would be highly desirable.

Aligned nanofibres offer a means of generating the physiological aligned neurites that interconnect cellular clusters *in vivo*[12]. Previous studies have demonstrated aligned nanofibres are capable of inducing aligned neurite extension for neurons cultured upon them, whether these neurons are primary cells, cell lines or differentiated from stem cells[13-18]. Somatic clustering is also required in order to represent a micro-circuit of the cerebral cortex. Limited adhesion of cells to the surface appears to

be crucial for producing an organoid; spinning bioreactors, hanging drop culture, suspension culture or low-adherence surfaces have all been employed as a means of limiting adhesion[10,11,19-23]. Limongi et al[24] suggested that there was an inverse relationship between cell-cell and cell-surface interactions. If low-adhesion cultures are a necessity in the generation of cerebral organoids, limiting cell-substratum interactions may promote 3D cell culture formation. Hydrophilic surfaces are used to maintain a dispersed monolayer of cells whilst hydrophobicity typically prevents cells from adhering to the substratum[25]. PLLA is a hydrophobic polymer that can be electrospun, can induce aligned neurite outgrowth and is frequently used for tissue engineering due to its biocompatibility and limited ability to generate an immune/inflammatory response[26-33]. Whilst a number of studies have utilised aligned PLLA nanofibres as a method of providing a 3D substrate for neuronal culture previously[13-16,34], several of these studies have employed neural stem cells/cell lines rather than primaries, PLLA nanofibres that have been treated with plasma, functional groups or bioactive molecules to increase their hydrophilicity and increase adhesion or primary dorsal root ganglion explants, and typically only performed morphological characterisation rather than molecular.

The aim of the current work was to combine two biomaterial properties that are known to induce desirable behaviours in cultured primary neurons (nanofibre alignment and hydrophobicity) and to determine if a more developed neuronal culture could be generated by culturing primary cortical neurons upon them.

2. Methods

2.1 Preparation of aligned PLLA nanofibre membranes

Aligned PLLA nanofibres were electrospun using a custom electrospinning set up to induce alignment [Patent number: GB2553316A[35]]. PLLA (Sigma-Aldrich Co Ltd, Poole, UK) was dissolved at 30% w/w in hexafluoroisopropanol (HFIP) (Sigma-Aldrich) overnight at 30°C. The solution was delivered at 1 ml/h to a 21 gauge stainless steel needle and subjected to an electric potential of 25 kV held between the needle and a grounded rotating collector drum spaced apart by 150 mm. Plasma treated PLLA

nanofibres (p-PLLA) were prepared by exposing aligned PLLA nanofibres to argon/oxygen plasma in a Plasmaline 415 Asher (CollabRx, Petaluma, USA) at 200 W for 5 minutes at a pressure of 200 mTorr. Narrow diameter (ND) PLLA nanofibres were prepared by increasing the distance between the needle and grounded rotating collector drum to 300 mm.

2.2 Characterisation of nanofibres

To quantify nanofibre diameter and morphology, PLLA, p-PLLA and narrow diameter (ND) nanofibres were coated in 5 nm of gold using a Q150R ES sputter coater (Quorum Technologies, Laughton, UK) prior to visualisation. A JSM-7100F scanning electron microscope (Jeol, Akishima, Japan), was used at an acceleration voltage of 10 kV. For each independent electrospin, 3 nanofibre membranes were utilised with 3 fields of view analysed for each membrane. Nanofibre alignment was measure using the Directionality Fiji plugin to determine the dispersion of nanofibre orientation under the described electrospinning parameters. Nanofibres were randomly selected for diameter quantification; 10 nanofibre diameters were measured for each field of view. Nanofibre diameters were measured using ImageJ (NIH) to determine the average nanofibre diameter using nanofibres produced from three independent electrospins.

Contact angles were measure using a Drop Shape Analyzer 10 MK2 (Kruss, Hamburg, Germany). Single drops of de-ionised water, each 5 µL in volume, were applied to the surface of aligned PLLA membranes and p-PLLA nanofibres and the contact angle was measured using a polynomial fit. Orientation of the membranes was consistent for each contact angles measurement, with 3 nanofibre membranes utilised for each of 3 replicates obtained from 3 independent electrospins.

For statistical testing of alterations to nanofibres, displayed in figure 3, one-way ANOVA was employed with Tukey's test used as a *post hoc* analysis.

2.3 Dissociation of primary cortical neurons

E18 Sprague Dawley cortices were provided by Brainbits UK (Long Eaton, UK). Tissue dissociation was performed using mechanical trituration using a silanised glass pipette after 10 minute incubation at 37°C in papain (0.5 mg/ml) (Sigma-Aldrich) dissolved in Ca^{2+}-free Hibernate-E medium (Brainbits). Cells were centrifuged at 200 × *g* for 90 seconds, resuspended in NBActiv1 medium (Brainbits) and a TC20 automated cell counter (BioRad, Watford, UK) was used to assess cell viability using Trypan Blue (Sigma-Aldrich) to count cells prior to plating at 25,000 cells/cm^2 in subsequent experiments. Media changes were performed every 7 days unless stated otherwise.

2.4 Cell Culture

Primary cortical neurons were seeded to aligned PLLA nanofibres. Cells were fixed in 4% (w/v) paraformaldehyde (Sigma-Aldrich), permeabilised in 0.1% (v/v) Triton X-100 (Sigma-Aldrich) and stained with anti-βIII tubulin (1:100) at 4°C (Santa-Cruz Biotechnology, Sc-51670) and secondary antibody (FITC-labelled anti-mouse IgG, 1:300) (Vector Laboratories, FI-2000) on 1, 3, 5, 7, 9 and 10 days *in vitro* (DIV). Reagents were diluted into PBS and incubations performed at room temperature unless stated otherwise. Images were taken on a Leica SP5 confocal microscope, using random sampling to reduce bias of quantification. Cluster diameter, neurite dispersion, neurite bundle diameter and neurite length were then quantified using ImageJ and used for regression analysis. Neurite dispersion was measured using the Directionality plugin of ImageJ. R^2 values and residual plots were calculated using GraphPad Prism 7.02. For each time point, 3 fields of vision and 3 replicates were used. After 10 DIV, 3 fields of vision were not employed as no neurons were detected other than those present within the cell cluster.

To determine mechanisms of self-assembly, dissociated primary cortical neurons were also seeded to p-PLLA nanofibres and ND aligned PLLA nanofibres, fixed, permeabilised and stained with anti-βIII-tubulin as described previously at 10 DIV. Student's t-test were used to determine morphological differences between the neurons cultured on PLLA and p-PLLA conditions described in figure 4.

2.5 Lactate dehydrogenase assay

Primary cortical neurons were plated on to aligned PLLA nanofibres. A 50 µL aliquot of culture supernatant was removed from each well on days 1, 7, 14, 21 and 28. Supernatants were transferred in to a 96-well plate and mixed with 50 µL of LDH reaction mixture (Thermo Fisher Scientific, Waltham, USA) and incubated at room temperature for 45 minutes. Stop solution (50 µL)was added and the resultant absorbance values were measured at 490 nm using a BMG Labtech Clariostar plate reader. Data are presented as a percentage of the control (absorbance value at D0) at each time point. One-way ANOVA was performed to ascertain the influence of the material on viability with Tukey's test used as *post hoc* analysis.

2.6 Preparation of lysates for mass spectrometry

For proteomic analysis, primary cortical neurons were seeded to aligned PLLA nanofibres as described previously and cultured for 14 days. Cells were then incubated for 2 minutes in lysis buffer (1/100 dilution of protease inhibitor cocktail (Sigma-Aldrich), 9.5 mM urea (Sigma-Aldrich), 130 mM dithiothreitol (Sigma-Aldrich) and 34 mM octyl-beta-glycopyranoside (Sigma-Aldrich) in ddH_2O) at 37°C. The cell lysate was then collected and sonicated in a water bath with ice 3 times for 5 minutes. Between sonication steps, samples were stored on ice for 5 minute rest periods. Samples were then centrifuged at 12,000 × *g* for 10 minutes and the supernatant was removed and frozen at -80°C until use.

2.7 Mass spectrometry

Lysates prepared from primary cortical neurons were diluted in tri-ethyl ammonium bicarbonate (Sigma-Aldrich) (50 mM) prior to reduction in DTT (5 mM) at 56°C for 20 minutes and alkylation in iodoacetamide (Sigma-Aldrich) (15 mM) at room temperature for 15 minutes in the dark. Lysates were then digested for 16 hours using trypsin at 37°C at a 20:1 protein:protease ratio (w/w) in a

thermomixer (650 rpm). Samples were then de-salted and concentration was performed using HyperSep C18 spin tips (10-200 µL size) using the manufacturer's protocol. A vacuum concentrator (Eppendorf, Hamburg, Germany) was then used to concentrate the samples before resuspension in 5 % (v/v) acetonitrile in 0.1 % (v/v) formic acid (Fluka Analytical, Buchs, Switzerland).

Samples were analysed using a Sciex TripleTOF 6600 mass spectrometer coupled in line with an eksigent ekspert nano LC 425 system running in micro flow. Samples (4 µL) were injected and trapped onto a YMC Triart-C18 pre-column (0.3 x 5 mm, 300 µm ID) (mobile phase A; 0.1 % (v/v) formic acid (Fluka Analytical), B; acetonitrile with 0.1 % (v/v) formic acid (Fluka Analytical)) at a flow rate of 10 µL/minute mobile phase A for 2 minutes prior to gradient elution onto the YMC Triart-C18 analytical column (15 cm, 3 µm, 300 µm ID) in line to a Sciex TripleTOF 6600 Duospray Source using a 5 µm electrode, positive mode +5500V. Initially, information dependent acquisition (IDA) mode was used to acquire a spectral library before using SWATH mode for data independent acquisition in order to generate quantitative data. The parameters for linear gradients used for IDA were as follows: mobile phase B increasing from 3 % to 30 % over 68 minutes; 40% B at 73 minutes. A column wash at 80 % B and re-equilibration was then performed (total run time = 87 minutes). The parameters for linear gradients used for SWATH were: 3-30 % B over 38 minutes; 40 % B at 43 minutes. Column wash and re-equilibration were performed as described previously (total run time = 57 minutes). For spectral library generation, IDA acquisition mode was utilised with a top 30 ion fragmentation (TOFMS m/z 400-1250; product ion 100-1500).

Exclusion was performed for 15 seconds using rolling collision energy, 50 ms accumulation time; 1.8 s cycle. For SWATH acquisition, 100 variable windows were used; 25 ms accumulation time, 2.6 s cycle (m/z 400-1250)[36]. ProteinPilot 5.0.2, iodoacetamide alkylation, thorough search with emphasis on biological modifications (Swissprot rat database June 2018) was used to search the IDA data whilst Sciex OneOmics software[37] extracted against the locally generated library (false discovery rate filtering of 1 % and excluding shared peptides) was used to analyse the SWATH data. Within the Sciex

OneOmics software, the parameters used were: 12 peptides per protein, 6 transitions per peptide, XIC width 30 ppm, 5 min retention time window.

2.8 Artificial neural network inference (ANNI) modelling

This approach was used for the simulation of protein-protein interactions based on confident and significant altered proteins generated through label-free quantitative mass spectrometry[38]. The use of ANNI enables the prediction of influence of all proteins among themselves and highlights their inter-relationship through the generation of interaction intensities for each protein with the remaining inputs. Generated interaction intensities can be positive and negative. Here, a 3-layered multi-layer perceptron with backpropagation learning and sigmoidal activation function was used[39]. Monte Carlo Cross-validation was applied to prevent overfitting using a randomly assigned 60:20:20 split for training, testing and validation.

Here, 186 proteins were analysed using ANNI resulting in the generation of 35 000 interactions. Selected proteins had confidence values greater than 50%; the confidence value cut-off was relaxed to generate a larger and more robust network. Interaction intensities were ranked by absolute interaction value. The top 100 most-influential interactions were selected and applied to Cytoscape (v3.6.0) for the visualisation of protein-protein interactions.

2.9 Network analysis

Significant interactions from the ANNI were input in to Cytoscape and the BiNGO plugin[40] was used to determine gene ontologies that were significantly overrepresented within the dataset, using a Hypergeometric test with a Benjamini and Hochberg False Discovery rate correction, set at a significance level of 0.05. “Developmental” gene ontologies were overrepresented within the network analysis and were selected for further analysis.

2. 10 Bioinformatic analysis

The 113 unique proteins that were identified with greater than 70% confidence that were significantly deregulated were enriched using Metacore. Three gene ontologies of interest were selected, "Developmental", "Synaptic", and "Adhesion". Heatmaps were generated for proteins that were classified in to each of these categories using Morpheus software or identified using the BiNGO plugin.

2.11 Validation of mass spectrometry by Western blot analysis

For this, protein lysates were prepared and quantified as described previously. Lysates were separated using SDS-PAGE and transferred onto nitrocellulose membrane filters. Membranes were incubated overnight in primary antibodies to either Vdac1 (Cell Signalling Technology, D73D12), Vdac2 (Abcam, ab37985) or HSP60 (Abcam, ab46798) diluted in in 3% w/v BSA in PBS. Blots were then incubated for 2 hours in secondary antibodies, consisting of horseradish peroxidase (HRP)-conjugated horse anti-mouse Ig (Cell Signalling Technology, 7076S) or goat anti- rabbit IgG (Cell Signalling Technology, 7074S) diluted in 3% (w/v) Marvel in PBS. Blots were developed with Pierce ECL Western blotting substrate (Thermo Fisher Scientific) and imaged using an ImageQuant Las 4000. Quantification was performed using Aida Image Analyzer v4.03 and protein loading was corrected against Vdac1, the housekeeper. Student's t-test was used to determine differences between the control and the nanofibre derived lysates.

2.12 Pharmacological stimulation of the 3D neuronal clusters

Primary cortical neurons were dissociated and cultured upon aligned PLLA nanofibres as described above for 14 days. At 14 DIV, neurons were washed with Hank's buffered saline solution (Thermo Fisher Scientific) three times and incubated for 15 minutes at room temperature with Fluovolt Membrane Potential Probe (Thermo Fisher Scientific), prepared according to the manufacturer's protocols (Thermo Fisher Scientific). Neurons were then washed three times in Hank's buffered saline solution and incubated in NbActiv1 medium (Brainbits). Plates were then loaded into a BMG Labtech Clariostar fluorescence plate reader and maintained in 5% CO_2 at 37°C. Recordings of fluorescence

intensity were taken every 60 milliseconds. At 12 and 26 seconds, automated injection of AMPA (10 µM) and GABA (25 µM) was performed. Raw data were converted in to Δ Fluorescence/Fluorescence (Δ F/F) for figures and subsequent statistical testing using ANOVA (GraphPad Prism 7) was applied to determine significant alterations in Δ F/F.

Spontaneous activity was also investigated using Fluovolt-loaded primary cortical neurons cultured on aligned PLLA nanofibres. Neurons were loaded as described previously and spontaneous fluorescence was quantified using a Leica SP5 confocal microscope. During quantification, cells were maintained at 37°C in an atmosphere of 5% CO_2.

3. Results

Culture of primary cortical neurons on aligned nanofibre membranes resulted in the rapid self-assembly of 3D cellular architectures. Clear compartmentalisation of the cell bodies could be observed, mimicking the gray matter of the brain more closely than the typical dispersed, random network that is observed for 2D primary neuronal cultures. Neurites extending from these clustered cell bodies were highly aligned and fasciculated. These 3D cellular architectures were confirmed to be stable up until 28 days and electrically active.

3.1 Characterisation of aligned poly-L-lactic acid nanofibres

Aligned PLLA nanofibres were generated using electrospinning. These nanofibres were electrospun as a membrane of highly aligned individual nanofibres (figure 1A) with a dispersion of 13±0.5° suggesting a high degree of alignment. The average diameter of the nanofibres was 858±57nm and the fibres displayed a smooth morphology (figure 1B).

3.2 Morphological analysis and viability of the 3D neuronal structures

A time-course experiment was run to demonstrate the self-assembly behaviours of the clusters rather than failure to dissociate (figure 1D-F). Over the time course, cell cluster size, neurite length and alignment were observed to increase, demonstrating progressive aggregation. By 10 DIV, neurites were aligned in the orientation of the nanofibres. Clusters were predominantly cylindrical, with an average width of 201±32 µm and an average length of 634±142 µm.

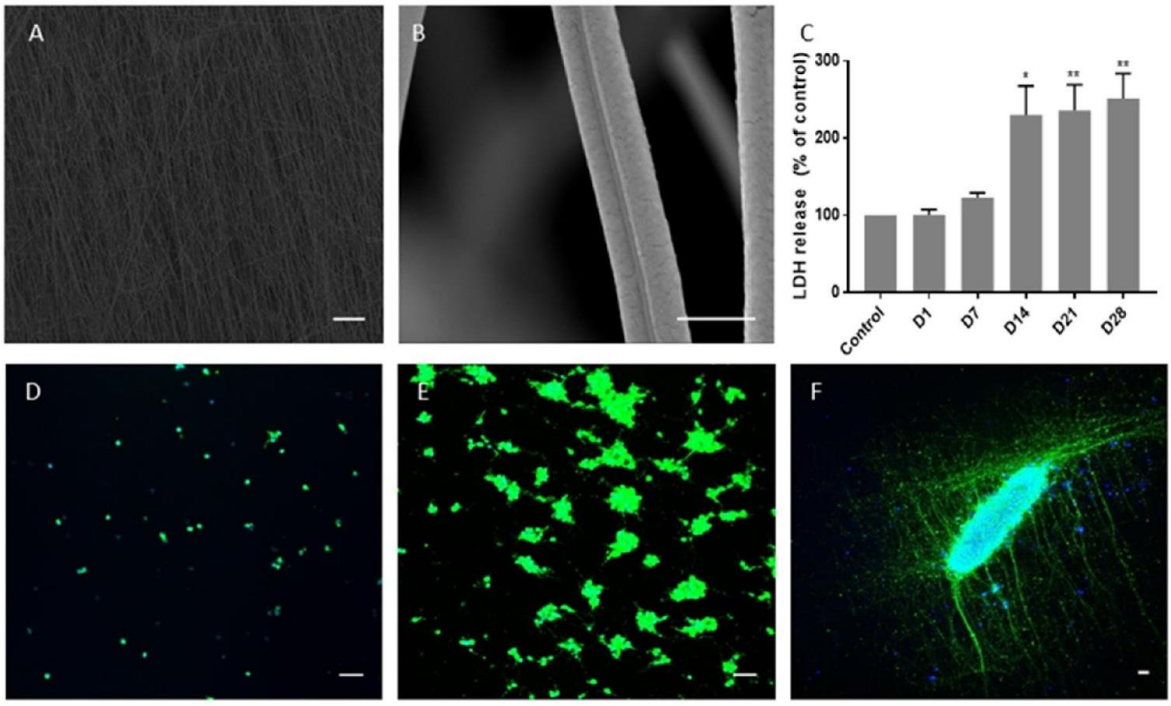

Figure 1: Characterisation of PLLA nanofibres and self-assembly of primary cortical neurons grown on a membrane of aligned PLLA nanofibres. For figures D-F, nanofibre alignment is consistent with the nanofibres displayed in figures A and B. Cells were stained with DAPI and anti-βIII tubulin. (A) x1,000 magnification scanning electron micrograph of PLLA nanofibres; average nanofibre diameter, 858±57nm, average nanofibre dispersion 13±0.4°. Scalebar = 100µm. (B) x25,000 magnification scanning electron micrograph of PLLA nanofibres, a smooth morphology is observed. Scale bar = 1µm. (C) Cell viability data shows that the organoids remain relatively stable for extended periods. A significant increase is observed between days 7 and 14 but after this point, cell viability remains stable (one-way ANOVA; n = 4, $F_{5,12}$ = 8.738, p = 0.0011). (D) At 1 DIV, neurons exhibit a typical, dispersed monolayer (E) At 5 DIV, cluster formation is evident yet directionality of neurite extension is low (F) At 10 DIV, self-assembly has occurred and the cell cluster has extended long, aligned neurites. Scale bar = 50µm

A significant increase in LDH release was observed for neurons cultured upon aligned PLLA nanofibre membranes (figure 1C, one-way ANOVA; $F_{5,12}$ = 8.738, p = 0.0011). No cytotoxic effect was observed for primary cultures as similar levels of lactate hydrogenase (LDH) were detected in culture medium between the control (absorbance at DIV0) and days 1 and 7 (Dunnett's multiple comparison test, q =

0.01597 and 0.6546, p = >0.999 and 0.9838 for DIV1 and DIV7 respectively). At DIV14, a significant elevation in LDH release was detected (Dunnett's multiple comparison test, q = 3.736, p = 0.0265) that was consistent at days DIV21 (Dunnett's multiple comparison test, q = 3.896, p = 0.0282) and DIV28 (Dunnett's multiple comparison test, q = 4.359 p = 0.0093), suggesting some cell death. However, no significant increase was found between DIV14 and DIV28 (Tukey's multiple comparison test, q = 0.8806, p = 0.9870).

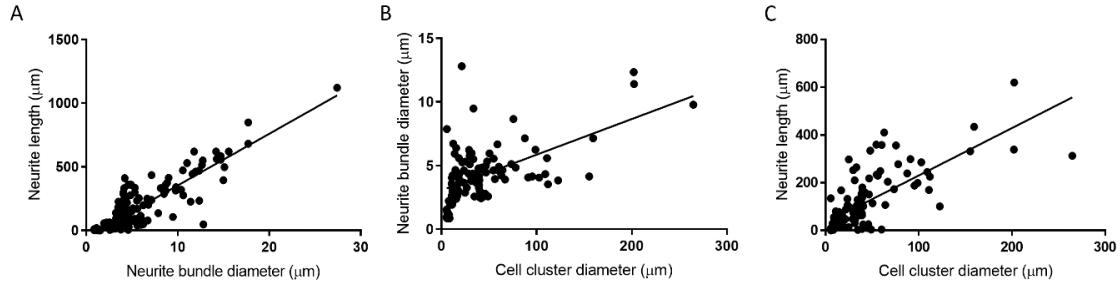

Figure 2: Correlation between neuronal morphological features for primary cortical neurons grown on aligned PLLA nanofibers, p = <0.0001 for all figures. Solid line indicates the regression line. (A) Correlation between neurite length and neurite bundle diameter (R^2 = 0.7599, n = 120). (B) Correlation between cell cluster diameter and neurite bundle diameter (R^2 = 0.3171, n = 93). (C) Correlation between the cell cluster diameter and neurite length (R^2 = 0.5301, n = 93).

Regression analysis was performed to ascertain the influence of the cell clustering on various neuronal structures (figure 2). A strong positive correlation was observed between neurite bundle diameter had a strong positive correlation with neurite length (R^2 = 0.7599, p <0.0001; figure 2A) while a positive correlation was observed between cell cluster diameter and neurite bundle diameter (R^2 = 0.3171, p <0.0001; figure 2B) and neurite length (R^2 = 0.5301, p<0.0001; figure 2C).

3.3 Elucidating the Mechanism of Self Assembly

PLLA was plasma treated in argon-oxygen plasma to reduce the hydrophobicity. As a result of the plasma treatment, pitting was observed (figure 3A) in the previously smooth surface of the nanofibres (figure 1B) and the wettability of the PLLA nanofibres was significantly enhanced (figure 3B) (t(16) = 26.44, p = <0.0001). When primary cortical neurons were cultured upon the plasma treated PLLA (p-PLLA) and cell clustering was not evident (figure 3C and 4A; t(21) = 23.38, p <0.0001) and the neurites

that extended from cells were less aligned (figure 4B; $t(12) = 4.56$, $p < 0.001$), thinner (figure 4C; $t(18) = 13.37$, $p < 0.0001$) and shorter (figure 4D; $t(18) = 14.12$, $p < 0.0001$).

A significant reduction was also observed in the diameter of the PLLA nanofibres upon plasma treatment ($F_{2,27} = 3.816$, $p < 0.0001$). Aligned PLLA nanofibres were electrospun to a smaller diameter ND PLLA, that was not significantly different from the hydrophilic p-PLLA nanofibres ($F_{2,27} = 3.816$, $p = 0.7970$) yet retained their hydrophobic properties although this was significantly lower than the control aligned PLLA nanofibres (contact angle = 131.9±2° and 112.3±0.66° for PLLA and ND PLLA respectively). One-way ANOVA, $F_{2,15} = 0.8935$, $p < 0.0001$). Neurons cultured on these nanofibres not only failed to form cell clusters but either did not survive or differentiate to neurons; cells on the narrow diameter nanofibres exhibited nuclear staining but did not express the neuronal marker (βIII-

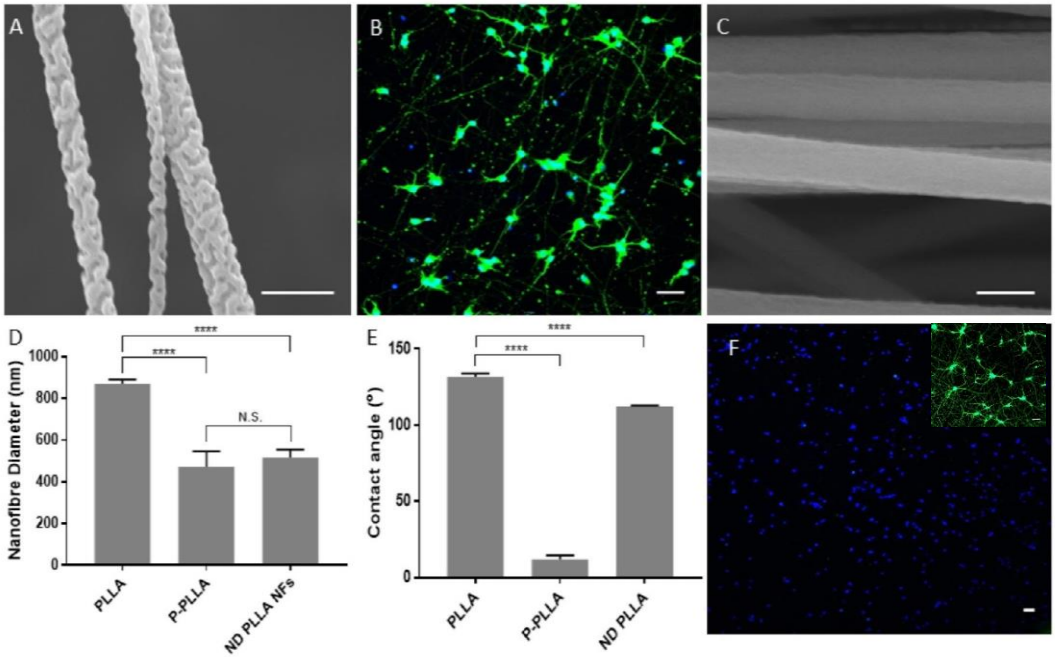

Figure 3: Determining the mechanism that induces formation of 3D cell clusters from primary cortical neurons (A) Plasma treated PLLA (p-PLLA) nanofibres displaying pitting. Scale bar = 1 µm (B) Primary cortical neurons grown on aligned p-PLLA nanofibres at 10 DIV display a significant reduction in neurite length (average length = 571 µm for untreated PLLA, 88.8 µm for p-PLLA. Student's t-test, n = 30; p value = <0.0001, t = 14.12, df = 18) and diameter (average neurite bundle diameter = 14.74 µm for untreated PLLA, 3.133 µm for p-PLLA. Student's t test; n = 30, p value = <0.0001, t = 13.37, df = 18) relative to neurons grown on untreated PLLA nanofibres. Scale bar = 50 µm. (C) Narrow diameter PLLA nanofibres (ND PLLA); no pitting is observed for narrow PLLA nanofibres. Scale bar = 1 µm. (D) Nanofibre diameter for untreated, plasma-treated and narrow diameter aligned PLLA nanofibres (870±20nm, 473±73nm and 517±38nm respectively. A significant reduction in diameter is observed for p-PLLA and narrow diameter nanofibres relative to the control (one-way ANOVA, Tukey's multiple comparison, n = 30; $F_{2,27}$ 3.816, p = <0.0001 for both) but were not significantly different from each other (one-way ANOVA, Tukey's multiple comparison, n = 30; $F_{2,27}$ 3.816, p = 0.7970). (E) Contact angles for untreated, plasma treated and narrow diameter aligned PLLA nanofibres (131.9±2°, 11.9±2.7° and 112.3±0.66° respectively), a significant reduction in contact angles is observed for plasma treated and narrow diameter nanofibres (one-way ANOVA, n = 16; $F_{2,15}$ = 0.8935, p = <0.0001 for both) (F) Culture of dissociated E18 cortical neurons on the narrow diameter NFs resulted in limited detection of neuronal marker βIII-tubulin despite the detection of the nuclear DAPI stain. The inset displays primary cortical neurons at an equivalent timepoint, grown in 2D culture. Scale bar = 50 µm.

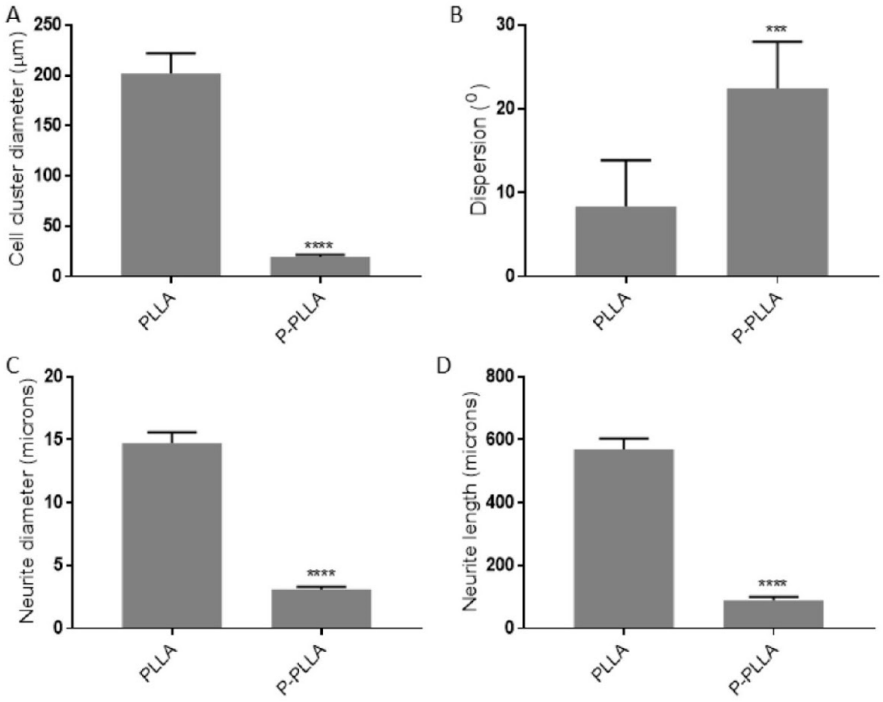

Figure 4: Changes to cortical neuronal behaviours induced by reducing the hydrophobicity. (A) Average diameter of cortical neuronal cell clusters that self-assembled on aligned PLLA and p-PLLA nanofibres (Student's t-test, n = 22; $t(21) = 23.38$, $p = <0.0001$). (B) Average dispersion of neurites grown on aligned PLLA and p-PLLA nanofibres (Student's t-test, n = 13; $t(12) = 4.56$, $p = 0.0007$); high dispersion is indicative of poor alignment. (C) Average neurite bundle diameter of neurites grown on aligned PLLA and p-PLLA nanofibres (Student's t-test, n = 19; $t(18) = 13.37$, $p = <0.0001$). (D) Hydrophobic PLLA nanofibres significantly increase the average length of neurites (Student's t-test, n = 19; $t(18) = 14.12$, $p = <0.0001$).

3.4 Proteomic Characterisation of the 3D Neuronal Clusters

Network analysis of the interactome generated by the ANN revealed many significantly enriched gene ontologies (table 2). The most significantly enriched gene ontologies related to "Development" (Hypergeometric test, (BiNGO software[40]: Nervous system development, $p = 0.000585$; Anatomical structure development, $p = 0.000661$; Multicellular organismal development, $p = 0.000661$; Developmental process, $p = 0.000925$; System development, $p = 0.00109$; Regulation of neuron projection development, $p = 0.00308$).

Gene Ontology Description	*p*-Value	Corrected *p*-Value	Cluster Frequency
Cellular process	2.46E-15	2.37E-12	56/74 75.6%
Localisation	7.62E-14	3.68E-11	31/74 41.8%
Transport	1.35E-13	3.99E-11	29/74 39.1%
Establishment of localization	1.65E-13	3.99E-11	29/74 39.1%
Establishment of localization in cell	3.76E-09	7.27E-07	13/74 17.5%

Cellular localisation	1.13E-08	1.81E-06	13/74 17.5%
Neurogenesis	1.52E-08	2.10E-06	13/74 17.5%
Multicellular organismal process	2.17E-08	2.62E-06	24/74 32.4%
Nervous system development	2.72E-08	2.92E-06	15/74 20.2%
Protein localization	4.98E-08	4.03E-06	13/74 17.5%
Macromolecule localization	5.15E-08	4.03E-06	14/74 18.9%
Biological regulation	5.28E-08	4.03E-06	40/74 54.0%
System development	5.72E-08	4.03E-06	21/74 28.3%
Anatomical structure development	5.85E-08	4.03E-06	22/74 29.7%
Developmental process	8.39E-08	5.16E-06	24/74 32.4%
Protein transport	8.55E-08	5.16E-06	12/74 16.2%
Establishment of protein localization	9.45E-08	5.37E-06	12/74 16.2%
Regulation of biological process	1.20E-07	6.42E-06	38/74 51.3%
Regulation of cellular component organization	1.72E-07	8.73E-06	10/74 13.5%
Regulation of cellular process	3.91E-07	1.89E-05	36/74 48.6%
Generation of neurons	6.10E-07	2.81E-05	11/74 14.8%
Regulation of cellular component size	6.94E-07	3.05E-05	7/74 9.4%
Intracellular transport	1.03E-06	4.32E-05	9/74 12.1%
Intracellular signaling pathway	2.58E-06	1.01E-04	12/74 16.2%

Table 2: The top 25 statistically overrepresented gene ontologies within the mass spectrometry dataset

Proteomic analysis of the neurons grown on the nanofibres revealed a shift in the proteomic profiles. Western blots were used to validate the mass spectrometry. VDAC2 and HSP60 expression were quantified (figure 5A) and the relative fold changes for each were compared to the values observed for mass spectrometry (figure 5B). VDAC2 exhibited a 2.11-fold upregulation ($p = 0.011$, $t(4) = 4.479$) while HSP60 exhibited a 3.09-fold change upregulation ($p = 0.0071$, $t(4) = 5.083$) as quantified by Western blot. For mass spectrometry, the observed upregulation for VDAC2 and HSP60 were 2.28 and 2.72 respectively. A marked reduction in the expression of proteins that were involved in adhesion was observed (figure 5C) whereas for synaptic proteins, an approximately equal number of proteins were up- and down-regulated (figure 5D). The majority of developmental proteins were upregulated (figure 5E); figure 5F displays ribosomal proteins which are downregulated during development.

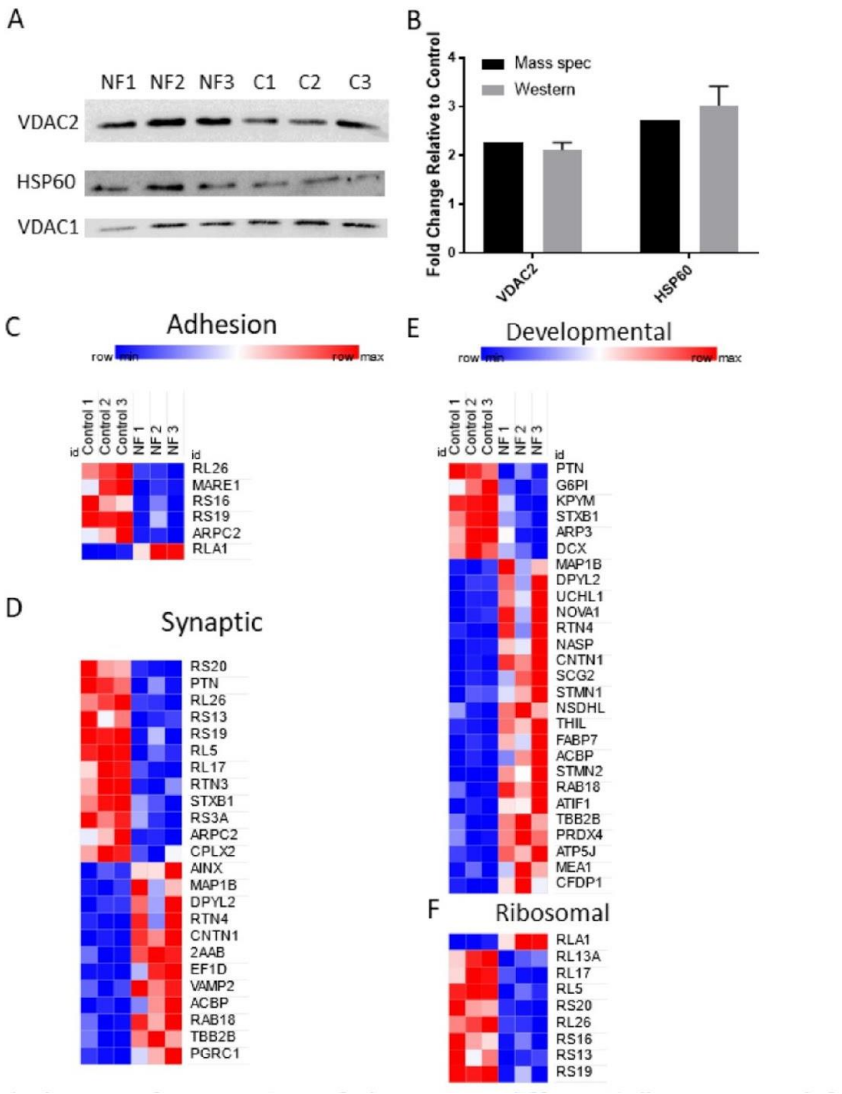

Figure 5: Fold changes for proteins that were differentially expressed for neurons grown on PLLA nanofibres relative to the 2D control. (A) Western blots for two of the proteins (HSP60; confidence value = 70%; VDAC2; confidence value = 56%) within the dataset alongside the housekeeper protein, VDAC1. Significant upregulation of HSP60 (Student's t-test, n = 3; p = 0.0071, t(4) = 5.083) and VDAC2 was observed for cortical neurons cultured on PLLA nanofibres (Student's t-test, n = 3; p = 0.011, t(4) = 4.479). (B) Normalised fold change values for mass spectrometry and Western blots for the selected proteins (C-E) Heat map visualization of fold change for selected gene ontologies as detected by mass spectrometry (n = 3) (red = increased expression, blue = decreased expression) (C) Adhesion (D) Synaptic (E) Developmental (F) Developmental - Ribosome

Analysis of the interactions of the identified proteins using an artificial neural network (ANN) indicated SNAP-25, reticulon-4 and DPYL2 as key mediators within the observed changes, with all other proteins exerting negative influence on these proteins to restore equilibrium within the system (figure 6). Two distinct networks appeared within the interactome. The first negatively regulates the expression of SNP25, a synaptic protein that is upregulated on the PLLA nanofibres. The second network displays a

greater degree of overlap as two upregulated proteins (Dpysl2 and Rtn4) are negatively influenced by the same range of proteins.

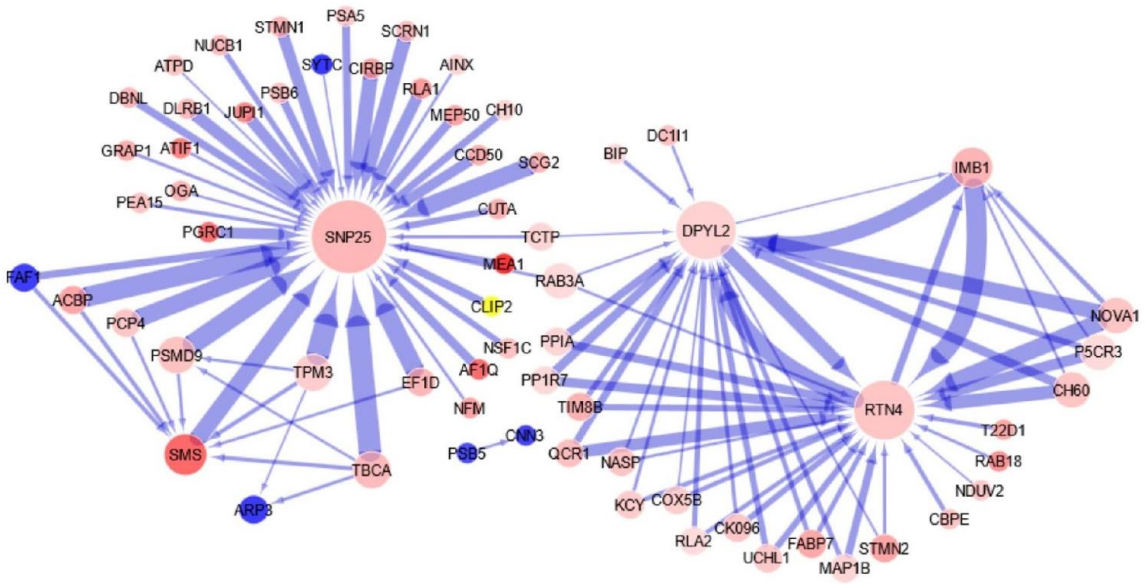

Figure 6: Artificial neural network inference (ANNI) of protein interactions. The strongest influencers that are up-/down-regulated by culture of primary cortical neurons on aligned PLLA nanofibres are displayed. The size of the node is relative to the number of interactions within the system. The colour of the node is dependent on the expression, red = increased expression, blue = decreased expression whilst the intensity is relative to the fold change. The arrows indicate the directionality of the influence. The colour of the arrows indicate the type of influence (red = positive influence, blue = negative influence) while the width of the arrow indicates the strength of the influence.

3.5 Response to pharmacological stimulation

Primary neurons cultured upon the aligned PLLA nanofibres demonstrated spontaneous spiking activity and responsiveness to a pharmacologically relevant agonist and antagonist, AMPA and GABA respectively (figure 7A; one way ANOVA: $F_{2,2055} = 1432$, $p < 0.0001$). A significant increase in Δ F/F was observed after administration of AMPA (Tukey's multiple comparison: $p < 0.0001$), an agonist to excitatory neurons, could be ameliorated by administration of GABA (Tukey's multiple comparison: $p < 0.0001$), an agonist to inhibitory neurons (figure 7B). Voltage changes were also quantified for spontaneous activity (figure 7C). At several points, the fluctuation in voltage exceeds a root mean square of 4, indicating signal 4 times greater than that of the noise, suggestive of spiking behaviour.

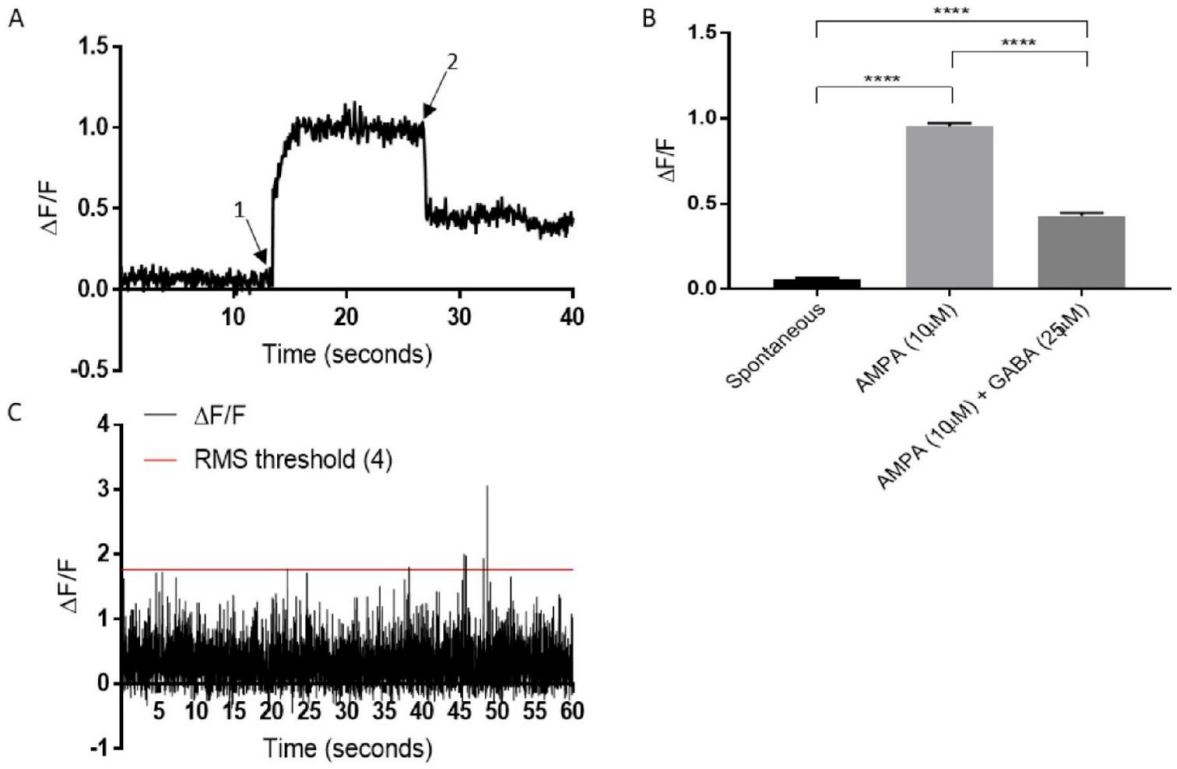

Figure 7: Fluovolt loaded 3D cell clusters generated using aligned PLLA nanofibres exhibit spontaneous and pharmacologically induced changes to membrane potential. (A) The averaged trace of 3 independent replicates. At approximately 13 seconds, AMPA (10 µM) is administered (1), resulting in an increase in membrane potential while GABA (25 µM) is administered at approximately 26 seconds (2), resulting in a decrease in membrane potential. (B) A significant difference was observed between each of the conditions ($F_{2,205}$ =1432, p = <0.0001) (C) Putative spontaneous spiking events were observed in the cell clusters; spikes were identified as datapoints that exceed 4 times the value of the root mean square (RMS). Sampling rate = 12 milliseconds.

4. Discussion

Aligned PLLA nanofibres were capable of inducing 3D neuronal architectures from a dispersed monolayer of primary cortical neurons within 10 days. The 3D neuronal architecture was composed of clustered cell bodies and aligned projections of fasciculated neurites extending an average of 634±142 µm from the cluster, although some heterogeneity was observed for the shape of the clusters. Whilst a significant increase was observed in LDH release at day 14, LDH levels in the culture medium remained consistent until 28 days. This is proposed to be due to a developmental apoptotic process; during development, both *in vivo* and *in vitro*, approximately 40% of cortical interneurons undergo apoptosis between days 11 and 18[41]. At 14 DIV, the same timepoint as the increase in cell death, neurons were demonstrated to be responsive to pharmacological agonists and exhibited

spontaneous spiking behaviours using a voltage sensitive dye, confirming that the 3D cell clusters were viable and exhibited some electrical activity, although further characterisation is needed to determine electrophysiological maturity relative to 2D cell culture. In conjunction with the LDH data, the activity at 14 DIV suggests that the cell clusters were stable until at least 28 days. On untreated PLLA nanofibres, correlations were noted between neurite morphology and the size of the clusters themselves, suggesting a role of cluster formation in the extensive neurite network that was observed (figure 2).

Whilst whole brain regions have been generated using stem cells[11,42], studies utilising primary cortical neurons that generate the desired neuronal architecture of compartmentalised cell bodies and neurites have required manual assembly via pelleting[43] or pre-made molds[44] to culture cells in. High concentrations of cells are typically employed[12,44,45] and whilst complex neurite arborisation is observed[45,12], control over the direction of neurite outgrowth is atypical[44]. In contrast, here the use of aligned hydrophobic nanofibres generated the desired neural architectures with relatively few cells (25,000 cells/cm^2) and controlled the directionality of the arborisation. While the work of Harris et al[43], Struzyna et al[45], Adewole et al[46] generated the desired architectures using their hydrogel based system, the clustered cell bodies were produced manually. The self-assembly of 3D cell clusters on aligned PLLA nanofibres contrasts the assembly methods of previous studies, minimising potentially detrimental handling of cells, whilst the methods of Kadoshima et al[11] and Lancaster et al[42] limit the cells to form in accordance with genetically pre-defined neuronal architectures.

4.1 Elucidating the mechanism for 3D neuronal architecture self-assembly

Inhibition of cell-substrate adhesion was suggested to be key for promoting organoid formation[19-23] and thus hydrophobicity was proposed as a mechanism for manipulating the adhesion of cells to the surface. For 2D primary neuronal cultures, the ability of cells to form clusters is inversely proportional

to the adherence of cells to the surface and the mechanical tension exerted by the neurites[47]. The mechanical tension exerted by neurites remains constant yet the force adhering the cells to the surface is proportional to the hydrophilicity of the surface[47]; thus on more hydrophobic surfaces, cells are more able to migrate and form clusters. However, the results indicate that hydrophobicity is not the only component that can influence cellular migration and the self-assembly behaviours of the cells.

The plasma treated hydrophilic nanofibres attenuated the migratory properties of the cells but had a significantly lower diameter than the control PLLA nanofibres (figure 3D); decreased diameter could play a role in the reduced adhesion of cells as neurons can wrap lamellopodia around narrow nanofibres[48]. Electrospun nanofibres that were hydrophobic and possessing a diameter that was not significantly different from the plasma treated nanofibres were prepared (ND nanofibres; figure 3C, 3D and 3E) but non-neuronal cells predominated the cultures (figure 3F). Reduction of nanofibre diameter increases the surface area and thus, degradation rate[49]; as PLLA degrades to lactic acid, it is possible that the reduction in nanofibre diameter induced cellular changes through lactic acid accumulation, inducing a shift in the sub-populations of cells within the culture. Several studies have shown a correlation between surface hydrophilicity and cell viability[50]; neurons cultured on the plasma treated nanofibres may have survived due to this factor but been prevented from aggregating due to the lack of hydrophobicity. Alternatively, the ND nanofibres may not have been hydrophobic enough as they were still significantly less hydrophobic than the control aligned PLLA nanofibres (figure 3E; one-way ANOVA; $F_{2,15} = 0.8935$, $p < 0.0001$). In addition, changes to the cellular microenvironment may be secondary to the biological changes induced by culture on the nanofibres; neurons cultured on the fibres show a decrease in expression of adhesive proteins (figure 5C). The exact mechanism responsible for the clustering appears to be a complex process that is at least partially dependent on hydrophobicity although other aspects appear to be involved.

4.2 Elucidating the mechanism for development of the cortical neurons

Due to the correlation that was observed between cell cluster size and the length/width of neurite bundles (figure 3), cell clustering was theorised to be a key factor in the development of the extensive neurite outgrowths and subsequent developmental molecular changes (figure 5). However, ANNI and bioinformatics analyses suggest that the changes are driven by the increased formation of synapses. The probability of synapse formation increases with decreasing inter-soma distance and when axons and dendrites pass within a threshold distance of each other[51,52]. Proteomic analysis confirmed the importance of synaptic proteins in the development of the structure. Of the three key nodes within the interactome (SNAP-25, Dpysl2 and Rtn4; figure 6) generated by ANNI, all 3 were detected in the list of synaptic proteins and two possessed a further function in development (Dpysl2 and Rtn4) (figure 5), suggesting that these 3 are key drivers in the development of the neuronal structure. Thus, the mechanism of 3D cell cluster formation is theorised to be limited adhesion, migration and subsequent soma cluster formation. The close proximity induces the formation of a greater number of synapses, increasing the expression of synaptic proteins which have a significant overlap of function with developmental proteins (figure 5), stimulating the development of the neurons.

4.3 Molecular Characterisation of the 3D Cellular Structures

Initial network analysis demonstrated that the most significantly overrepresented gene ontologies were developmental gene ontologies (figure 5). Proteins that are downregulated as a result of culturing neurons on the PLLA nanofibres include proteins that play a role in neurogenesis but decrease as neurons mature (Dcx[53,54]) and play a role in neurite initiation and arborisation (Stxbp1 and Marcks[55,58]). Notably, mass downregulation of the ribosomal proteins was observed (figure 5F); ribosomal protein downregulation has recently been observed to occur during development of the forebrain[59]. In contrast, upregulated proteins had notable roles in lamination of the cerebral cortex, for example Rab18, Dpysl2, Tubb2B, Ncan, DBNL, Tuba1A, Rtn4, Rab5a and Stmn2[60-64], axon fasciculation, guidance and growth (CNTN1, Ncan, Tubb3[60,65,66]) and polarisation (DBNL, Dpysl2[62,64]).

These results suggest that the 3D cellular structures are more similar to their *in vivo* counterparts than the 2D control at a proteomic level.

4.4 Limitations to using aligned PLLA nanofibres to generate 3D cortical structures

The reliance on axonal tension as a means of self-assembly[47] may explain the homoaggregation that occurs; all cells within the clusters were neuronal. Cells that stained for DAPI but did not stain for βIII-tubulin were present and localised external to the structure. Whilst this demonstrates that the culture can support the survival of non-neuronal cells as part of a non-contact co-culture, it represents a limitation of using the PLLA nanofibres for generating a mixed 3D neuronal culture. Whilst this cluster may appear to be more structurally representative of the *in vivo* cortex than a conventional 2D culture, incorporating glial cells into the structure to form a heteroaggregate will be key to developing the 3D neuronal cluster to an organoid[9]. The absence of integrated glial populations within our research has been overcome by Lancaster et al[42] and Kadoshima et al[11] via differentiation of stem cells to terminally differentiated glia. It is possible that by combining the differentiation protocols with the aligned PLLA nanofibre structures described within this paper, the absence of glial populations can be prevented. In addition, the size of the 3D cellular structure will be limited by the range of oxygen and nutrient diffusion into the tissue in the absence of well-developed vasculature[10].

4.5 Future implications

This facile method of culturing 3D neuronal cultures has implications for numerous fields. Due to the simplicity of the protocol and the speed of generating the structure relative to other methods[10,11], the 3D culture could be employed for high throughput assays as a method of reducing the number of animals required to generate organotypic slices. The cell clusters could also be used to study developmental processes such as neurite fasciculation, neurite outgrowth or dendritic spine formation within fasciculated bundles. With the ability to specify the directionality of the neurite

extension due to contact guidance along the nanofibres, several of these cell clusters could be complexed to represent neural circuitry *in vitro* in a similar manner to the methods of Peyrin et al[67], Kanagasabapathi et al[68] and Berdichevsky et al[69], although these methods mimicked the connections between two pathways exclusively in 2D culture. Serruya et al[70] generated 3D cell clusters and aligned neurites encapsulated within an agarose shell and proposed their use to repair damaged pathways or as sensors for a brain-machine interface, re-routing connections from deep brain regions to the surface, thus reducing the invasiveness of recording electrodes. A key factor enabling such advances is that the cell clusters are grown on PLLA which, unlike several biomaterial polymers, is known to be highly biocompatible in an *in vivo* setting. Thus, the methods outlined here could also be used to develop similar neural implants for use in brain repair.

5. Conclusions

The work describes a facile method of culturing primary cortical neurons to generate a homogenous, electrically active cortical neuronal cluster with predominantly aligned neurites. These neuronal clusters exhibit an upregulation of proteins that are involved in cortical lamination, polarisation and maturity, suggesting that from a molecular perspective, they are more developed and physiological than their 2D counterparts. Untreated PLLA nanofibres show promise for advanced 3D cell culture due to their biocompatibility and promotion of the self-assembly of these 3D neuronal structures. Due to the increasing use of 3D cell culture for pharmaceutical uses and developmental research, it would be highly advantageous to extend the applicability of these approaches by producing *in vitro* neural architectures using self-renewing cells as well as primary neurons.

Acknowledgements

The authors would like to thank Nottingham Trent University for funding the study.

References

[1] Irons, H.R.; Cullen, D.K.; Shapiro, N.P.; Lambert, N.A.; Lee, R.H.; LaPlaca, M.C. Three-dimensional

neural constructs: a novel platform for neurophysiological investigation. *J. Neural Eng.* **2008**, *5*(3), 333-341. DOI: 10.1088/1741-2560/5/3/006

[2] Flanagan, L.A.; Ju, Y.E.; Marg, B.; Osterfield, M.; Janmey, P.A. Neurite branching on deformable substrates. *Neuroreport* **2002**, *13*(18), 2411-2415. DOI: 10.1097/01.wnr.0000048003.96487.97

[3] Saha, K.; Keung, A.J.; Irwin, E.F.; Li, Y.; Little, L.; Schaffer, D.V.; Healy, K.E. Substrate modulus directs neural stem cell behavior. *Biophys. J.* ***2008***, *95*(9), 4426-4438. DOI: 10.1529/biophysj.108.132217.

[4] Koser, D.E.; Thompson, A.J.; Foster, S.K.; Dwivedy, A.; Pillai, E.K.; Sheridan, G.K.; Svoboda, H.; Viana, M.; da F Costa, L.; Guck, J.; Holt, C.E. Mechanosensing is critical for axon growth in the developing brain. *Nat. Neurosci.* **2016**, *19*(12), 1592-1598. DOI: 10.1038/nn.4394.

[5] Prabhakaran, M.P.; Ghasemi-Mobarakeh, L.; Jin, G.; Ramakrishna, S. Electrospun conducting polymer nanofibers and electrical stimulation of nerve stem cells. *J. Biosci. Bioeng.* **2011**, *112*(5), 501-507. DOI: 10.1016/j.jbiosc.2011.07.010.

[6] Feng, Z.Q.; Wang, T.; Zhao, B.; Li, J.; Jin, L. Soft graphene nanofibers designed for the acceleration of nerve growth and development. *Adv. Mater.* **2015**, 27(41), 6462-6468. DOI: 10.1002/adma.201503319

[7] Choi, A.; Kim, J.Y.; Lee, J.E.; Jung, H.I. Effects of PDMS curing ratio and 3D micro-pyramid structure on the formation of an in vitro neural network. *Curr. Appl. Phys.* **2009**, *9*(4), e294-e297. DOI: 10.1016/j.cap.2009.06.029.

[8] Fatehullah, A.; Tan, S.H.; Barker, N. Organoids as an in vitro model of human development and disease. *Nat. Cell Biol.* **2016,** *18*(3), 246-254. DOI: 10.1038/ncb3312

[9] Chambers, S.M.; Tchieu, J.; Studer, L. Build-a-brain, *Cell Stem Cell* **2013**, *13*(4), 377-378. DOI: 10.1016/j.stem.2013.09.010

[10] Lancaster, M.A.; Knoblich, J.A. Generation of cerebral organoids from human pluripotent stem cells. *Nat. Protoc.* **2014**, *9*(10), 2329-2340. DOI: 10.1038/nprot.2014.158

[11] Kadoshima, T.; Sakaguchi, H.; Nakano, T.; Soen, M.; Ando, S.; Eiraku, M.; Sasai, Y. Self-organization of axial polarity, inside-out layer pattern, and species-specific progenitor dynamics in human ES cell–derived neocortex. *Proc. Natl. Acad. Sci. U. S. A.* **2013**, *110*(50), 20284-20289. DOI: 10.1073/pnas.1315710110

[12] Tang-Schomer, M.D.; White, J.D.; Tien, L.W.; Schmitt, L.I.; Valentin, T.M.; Graziano, D.J.; Hopkins, A.M.; Omenetto, F.G.; Haydon, P.G.; Kaplan, D.L. Bioengineered functional brain-like cortical tissue. *Proc. Natl. Acad. Sci. U. S. A.* **2014,** *11*(38), 13811-13816. DOI: 10.1073/pnas.1324214111

[13] Corey, J.M.; Gertz, C.C.; Wang, B.S.; Birrell, L.K.; Johnson, S.L.; Martin, D.C.; Feldman, E.L. The design of electrospun PLLA nanofiber scaffolds compatible with serum-free growth of primary motor and sensory neurons. *Acta biomater.* **2008,** *4*(4), 863-875. DOI: 10.1016/j.actbio.2008.02.020

[14] Yang, F.; Murugan, R.; Wang, S.; Ramakrishna, S. Electrospinning of nano/micro scale poly (L-lactic acid) aligned fibers and their potential in neural tissue engineering. *Biomaterials* **2005**, *26*(15), 2603-2610. DOI: 10.1016/j.biomaterials.2004.06.051

[15] Xie, J.; MacEwan, M.R.; Li, X.; Sakiyama-Elbert, S.E.; Xia, Y. Neurite outgrowth on nanofiber scaffolds with different orders, structures, and surface properties. *ACS nano* **2009**, *3*(5), 1151-1159. DOI: 10.1021/nn900070z

[16] Koh, H.S.; Yong, T.; Chan, C.K.; Ramakrishna, S. Enhancement of neurite outgrowth using nano-structured scaffolds coupled with laminin. *Biomaterials* **2008**, *29*(26), 3574-3582. DOI: 10.1016/j.biomaterials.2008.05.014.

[17] Luo, B.; Tiwari, A.P.; Chen, N.; Ramakrishna, S.; Yang, I.H. Development of an Axon-Guiding Aligned Nanofiber-Integrated Compartmentalized Microfluidic Neuron Culture System. *ACS Appl. Bio Mater.* **2021,** 4(12), 8424-8432. DOI: 10.1021/acsabm.1c00960.

[18] Zhang, K.; Zheng, H.; Liang, S.; Gao, C. Aligned PLLA nanofibrous scaffolds coated with graphene oxide for promoting neural cell growth. *Acta Biomater.* **2016**, *37*, 131-142. DOI: 10.1016/j.actbio.2016.04.008.

[19] Camp, J.G.; Badsha, F.; Florio, M.; Kanton, S.; Gerber, T.; Wilsch-Bräuninger, M.; Lewitus, E.; Sykes, A.; Hevers, W.; Lancaster, M.; Knoblich, J.A. Human cerebral organoids recapitulate gene expression programs of fetal neocortex development. *Proc. Natl. Acad. Sci. U. S. A.* **2015**, 112(51), 15672-15677. DOI: 10.1073/pnas.1520760112

[20] Dang, J.; Tiwari, S.K.; Lichinchi, G.; Qin, Y.; Patil, V.S.; Eroshkin, A.M.; Rana, T.M. Zika virus depletes neural progenitors in human cerebral organoids through activation of the innate immune receptor TLR3. *Cell stem cell* **2016**, *19*(2), 258-265. DOI: 10.1016/j.stem.2016.04.014

[21] Bershteyn, M.; Nowakowski, T.J.; Pollen, A.A.; Di Lullo, E.; Nene, A.; Wynshaw-Boris, A.; Kriegstein, A.R. Human iPSC-derived cerebral organoids model cellular features of lissencephaly and reveal prolonged mitosis of outer radial glia. *Cell stem cell* **2017**, 20(4), 435-449. DOI: 10.1016/j.stem.2016.12.007

[22] Ogawa, J.; Pao, G.M.; Shokhirev, M.N.; Verma, I.M. Glioblastoma model using human cerebral organoids. *Cell rep.* **2018**, *23*(4), 1220-1229. DOI: 10.1016/j.celrep.2018.03.105

[23] Allende, M.L.; Cook, E.K.; Larman, B.C.; Nugent, A.; Brady, J.M.; Golebiowski, D.; Sena-Esteves, M.; Tifft, C.J.; Proia, R.L. Cerebral organoids derived from Sandhoff disease-induced pluripotent stem cells exhibit impaired neurodifferentiation. *J. Lipid Res.* **2018**, 59 (3), 550-563. DOI: 10.1194/jlr.M081323

[24] Limongi, T.; Cesca, F.; Gentile, F.; Marotta, R.; Ruffilli, R.; Barberis, A.; Dal Maschio, M.; Petrini, E.M.; Santoriello, S.; Benfenati, F.; Di Fabrizio, E. Nanostructured superhydrophobic substrates trigger the development of 3D neuronal networks. *Small* **2013**, *9*(3), 402-412. DOI: 10.1002/smll.201201377

[25] Ryan, J.A. Evolution of cell culture surfaces. *BioFiles* **2008**, *3*(8), 21

[26] Evans, G.R.; Brandt, K.; Niederbichler, A.D.; Chauvin, P.; Hermann, S.; Bogle, M.; Otta, L.; Wang, B.; Patrick, C.W. Clinical long-term in vivo evaluation of poly (L-lactic acid) porous conduits for peripheral nerve regeneration. *J. Biomater. Sci., Polym. Ed.* **2000***, Polymer Edition*, *11*(8), 869-878. DOI: 10.1163/156856200744066

[27] Evans, G.R.D.; Brandt, K.; Widmer, M.S.; Lu, L.; Meszlenyi, R.K.; Gupta, P.K.; Mikos, A.G.; Hodges, J.; Williams, J.; Gürlek, A.; Nabawi, A. In vivo evaluation of poly (L-lactic acid) porous conduits for peripheral nerve regeneration. *Biomaterials* **1999**, *20*(12), 1109-1115. DOI: 10.1016/s0142-9612(99)00010-1

[28] Koh, H.S.; Yong, T.; Teo, W.E.; Chan, C.K.; Puhaindran, M.E.; Tan, T.C.; Lim, A.; Lim, B.H.; Ramakrishna, S. In vivo study of novel nanofibrous intra-luminal guidance channels to promote nerve regeneration. *J. Neural Eng.* **2010**, *7*(4), 046003. DOI: 10.1088/1741-2560/7/4/046003

[29] Jaiswal, A.K.; Dhumal, R.V.; Bellare, J.R.; Vanage, G.R. In vivo biocompatibility evaluation of electrospun composite scaffolds by subcutaneous implantation in rat. *Drug Delivery Transl. Res.* **2013**, *3*(6), 504-517. DOI: 10.1007/s13346-013-0153-z

[30] Hwang, D.W.; Jin, Y.; Lee, D.H.; Kim, H.Y.; Cho, H.N.; Chung, H.J.; Park, Y.; Youn, H.; Lee, S.J.; Lee, H.J.; Kim, S.U. In vivo bioluminescence imaging for prolonged survival of transplanted human neural stem cells using 3D biocompatible scaffold in corticectomized rat model. *PloS one* **2014**, *9*(9), p.e105129. DOI: 10.1371/journal.pone.0105129

[31] Rivet, C.J.; Zhou, K.; Gilbert, R.J.; Finkelstein, D.I.; Forsythe, J.S. Cell infiltration into a 3D electrospun fiber and hydrogel hybrid scaffold implanted in the brain. *Biomatter* **2015**, *5*(1), p.e1005527. DOI: 10.1080/21592535.2015.1005527

[32] Wang, T.Y.; Bruggeman, K.F.; Kauhausen, J.A.; Rodriguez, A.L.; Nisbet, D.R.; Parish, C.L. Functionalized composite scaffolds improve the engraftment of transplanted dopaminergic progenitors in a mouse model of Parkinson's disease. *Biomaterials* **2016**, *74*, 89-98. DOI: 10.1016/j.biomaterials.2015.09.039

[33] Li, Z.; Zhang, X.; Ouyang, J.; Chu, D.; Han, F.; Shi, L.; Liu, R.; Guo, Z.; Gu, G.X.; Tao, W.; Jin, L. Ca2+-supplying black phosphorus-based scaffolds fabricated with microfluidic technology for osteogenesis. *Bioactive materials* **2021**, *6*(11), 4053-4064. DOI: 10.1016/j.bioactmat.2021.04.014.

[34] Marote, A.; Barroca, N.; Vitorino, R.; Silva, R.M.; Fernandes, M.H.; Vilarinho, P.M.; e Silva, O.A.D.C.; Vieira, S.I. A proteomic analysis of the interactions between poly (L-lactic acid) nanofibers and SH-SY5Y neuronal-like cells. *AIMS Mol. Sci.* **2016**, *3*(4), 661-682. DOI: 10.3934/molsci.2016.4.661

[35] Chemmarappally, J.M.; Pegram, H.C.; Abeywickrama, N.; Fornari, E.; Hargreaves, A.J.; De Girolamo, L.A.; Stevens, B. A Co-Culture nanofibre scaffold model of neural cell degeneration in relevance to Parkinson's disease. *Sci. Rep.* **2020**, *10*(1), 1-14. DOI: 10.1038/s41598-020-59310-x

[36] Mele, L.; Paino, F.; Papaccio, F.; Regad, T.; Boocock, D.; Stiuso, P.; Lombardi, A.; Liccardo, D.; Aquino, G.; Barbieri, A.; Arra, C. A new inhibitor of glucose-6-phosphate dehydrogenase blocks pentose phosphate pathway and suppresses malignant proliferation and metastasis in vivo. *Cell Death Dis.* **2018**, *9*(5), 1-12. DOI: 10.1038/s41419-018-0635-5

[37] Lambert, J.P.; Ivosev, G.; Couzens, A.L.; Larsen, B.; Taipale, M.; Lin, Z.Y.; Zhong, Q.; Lindquist, S.; Vidal, M.; Aebersold, R.; Pawson, T. Mapping differential interactomes by affinity purification coupled with data-independent mass spectrometry acquisition. *Nat. Methods* **2013**, *10*(12), 1239-1245. DOI: 10.1038/nmeth.2702

[38] Tong, D.L.; Boocock, D.J.; R. Dhondalay, G.K.; Lemetre, C.; Ball, G.R. Artificial neural network inference (ANNI): a study on gene-gene interaction for biomarkers in childhood sarcomas. *PLoS One* **2014**, *9*(7), p.e102483. DOI: 10.1371/journal.pone.0102483

[39] Lancashire, L.J.; Lemetre, C.; Ball, G.R. An introduction to artificial neural networks in bioinformatics—application to complex microarray and mass spectrometry datasets in cancer studies. *Briefings Bioinfo.* **2009**, *10*(3), 315-329. DOI: 10.1093/bib/bbp012

[40] Maere, S.; Heymans, K.; Kuiper, M. BiNGO: a Cytoscape plugin to assess overrepresentation of gene ontology categories in biological networks. *Bioinformatics* **2005**, *21*(16), 3448-3449. DOI: 10.1093/bioinformatics/bti551

[41] Southwell, D.G.; Paredes, M.F.; Galvao, R.P.; Jones, D.L.; Froemke, R.C.; Sebe, J.Y.; Alfaro-Cervello, C.; Tang, Y.; Garcia-Verdugo, J.M.; Rubenstein, J.L.; Baraban, S.C. Intrinsically determined cell death of developing cortical interneurons. *Nature* **2012**, *491*(7422), 109-113. DOI: 10.1038/nature11523

[42] Lancaster, M.A.; Renner, M.; Martin, C.A.; Wenzel, D.; Bicknell, L.S.; Hurles, M.E.; Homfray, T.; Penninger, J.M.; Jackson, A.P.; Knoblich, J.A. Cerebral organoids model human brain development and microcephaly. *Nature* **2013**, *501*(7467), 373-379. DOI: 10.1038/nature12517

[43] Harris, J.P.; Struzyna, L.A.; Murphy, P.L.; Adewole, D.O.; Kuo, E.; Cullen, D.K. Advanced biomaterial strategies to transplant preformed micro-tissue engineered neural networks into the brain. *J. Neural Eng.* **2016**, *13*(1), p016019. DOI: 10.1088/1741-2560/13/1/016019

[44] Kato-Negishi, M.; Morimoto, Y.; Onoe, H.; Takeuchi, S. Millimeter-Sized Neural Building Blocks for 3D Heterogeneous Neural Network Assembly. *Adv. Healthc. Mater.* **2013**, *2*(12), 1564-1570. DOI: 10.1002/adhm.201300052

[45] Struzyna, L.A.; Browne, K.D.; Brodnik, Z.D.; Burrell, J.C.; Harris, J.P.; Chen, H.I.; Wolf, J.A.; Panzer, K.V.; Lim, J., Duda, J.E.; España, R.A. Tissue engineered nigrostriatal pathway for treatment of Parkinson's disease. *J. Tissue Eng. Regener. Med.* **2018**, *12*(7), 1702-1716. DOI: 10.1002/term.2698

[46] Adewole, D.O.; Struzyna, L.A.; Burrell, J.C.; Harris, J.P.; Nemes, A.D.; Petrov, D.; Kraft, R.H.; Chen, H.I.; Serruya, M.D.; Wolf, J.A.; Cullen, D.K. Development of optically controlled “living electrodes” with long-projecting axon tracts for a synaptic brain-machine interface. *Sci. Adv.* **2021**, *7*(4), p.eaay5347. DOI: 10.1126/sciadv.aay5347

[47] Segev, R.; Benveniste, M.; Shapira, Y.; Ben-Jacob, E. Formation of electrically active clusterized neural networks. *Phys. Rev. Lett.* **2003**, *90*(16), p.168101. DOI: 10.1103/PhysRevLett.90.168101

[48] Kueh, J.L.L.; Li, D.; Raisman, G.; Jenkins, D.; Li, Y.; Stevens, R. Directionality and bipolarity of olfactory ensheathing cells on electrospun nanofibers. *Nanomedicine* **2012**, *7*(8), 1211-1224. DOI: 10.2217/nnm.11.180

[49] Dahlin, R.L.; Kasper, F.K.; Mikos, A.G. Polymeric nanofibers in tissue engineering. *Tissue Eng., Part B* **2011**, *17*(5), 349-364. DOI: 10.1089/ten.TEB.2011.0238

[50] Schaub, N.J.; Le Beux, C.; Miao, J.; Linhardt, R.J.; Alauzun, J.G.; Laurencin, D.; Gilbert, R.J. The effect of surface modification of aligned poly-L-lactic acid electrospun fibers on fiber degradation and neurite extension. *PLoS One* ***2015***, *10*(9), p.e0136780. DOI: 10.1371/journal.pone.0136780

[51] Perin, R.; Berger, T.K.; Markram, H. A synaptic organizing principle for cortical neuronal groups. *Proc. Natl. Acad. Sci. U. S. A.* **2011**, *108*(13), 5419-5424. DOI: 10.1073/pnas.1016051108

[52] van Ooyen, A.; Carnell, A.; de Ridder, S.; Tarigan, B.; Mansvelder, H.D.; Bijma, F.; de Gunst, M.; van Pelt, J. Independently outgrowing neurons and geometry-based synapse formation produce networks with realistic synaptic connectivity. *PloS one* **2014**, *9*(1), p.e85858. DOI: 10.1371/journal.pone.0085858

[53] Fang, P.; Schachner, M.; Shen, Y.Q. HMGB1 in development and diseases of the central nervous system. *Mol. Neurobiol.* **2012**, *45*(3), 499-506. DOI: 10.1007/s12035-012-8264-y

[54] Dhaliwal, J.; Xi, Y.; Bruel-Jungerman, E.; Germain, J.; Francis, F.; Lagace, D.C. Doublecortin (DCX) is not essential for survival and differentiation of newborn neurons in the adult mouse dentate gyrus. *Front. Neurosci.* **2016**, *9*, p.494. DOI: 10.3389/fnins.2015.00494

[55] Broeke, J.H.; Roelandse, M.; Luteijn, M.J.; Boiko, T.; Matus, A.; Toonen, R.F.; Verhage, M. Munc18 and Munc13 regulate early neurite outgrowth. *Biol. Cell* **2010**, *102*(8), 479-488. DOI: 10.1042/BC20100036

[56] Leondaritis, G.; Eickholt, B.J. Short lives with long-lasting effects: filopodia protrusions in neuronal branching morphogenesis. *PLoS Biol.* **2015**, *13*(9), p.e1002241. DOI: 10.1371/journal.pbio.1002241

[57] Hamada, N.; Iwamoto, I.; Tabata, H.; Nagata, K.I. MUNC18–1 gene abnormalities are involved in neurodevelopmental disorders through defective cortical architecture during brain development. *Acta Neuropathol. Commun.* **2017**, *5*(1), 1-16. DOI: 10.1186/s40478-017-0498-5

[58] Brudvig, J.J.; Cain, J.T.; Sears, R.M.; Schmidt-Grimminger, G.G.; Wittchen, E.S.; Adler, K.B.; Ghashghaei, H.T.; Weimer, J.M. MARCKS regulates neuritogenesis and interacts with a CDC42 signaling network. *Sci. Rep.* **2018**, *8*(1), 1-11. DOI: 10.1038/s41598-018-31578-0

[59] Chau, K.F.; Shannon, M.L.; Fame, R.M.; Fonseca, E.; Mullan, H.; Johnson, M.B.; Sendamarai, A.K.; Springel, M.W.; Laurent, B.; Lehtinen, M.K. Downregulation of ribosome biogenesis during early forebrain development. *Elife* **2018**, *7*, p.e36998. DOI: 10.7554/eLife.36998.001

[60] Inatani, M.; Honjo, M.; Otori, Y.; Oohira, A.; Kido, N.; Tano, Y.; Honda, Y.; Tanihara, H. Inhibitory effects of neurocan and phosphacan on neurite outgrowth from retinal ganglion cells in culture. *Invest. Ophthalmol. Visual Sci.* **2001**, *42*(8), 1930-1938.

[61] Jaglin, X.H.; Poirier, K.; Saillour, Y.; Buhler, E.; Tian, G.; Bahi-Buisson, N.; Fallet-Bianco, C.; Phan-Dinh-Tuy, F.; Kong, X.P.; Bomont, P.; Castelnau-Ptakhine, L. Mutations in the β-tubulin gene TUBB2B result in asymmetrical polymicrogyria. *Nat. Genet.* **2009**, *41*(6), 746-752. DOI: 10.1038/ng.380

[62] Ip, J.P.; Fu, A.K.; Ip, N.Y. CRMP2: functional roles in neural development and therapeutic potential in neurological diseases. *The Neuroscientist* ***2014***, *20*(6), 589-598. DOI: 10.1177/1073858413514278

[63] Wu, Q.; Sun, X.; Yue, W.; Lu, T.; Ruan, Y.; Chen, T.; Zhang, D. RAB18, a protein associated with Warburg Micro syndrome, controls neuronal migration in the developing cerebral cortex. *Mol. brain* **2016**, *9*(1), 1-12. DOI: 10.1186/s13041-016-0198-2

[64] Inoue, S.; Hayashi, K.; Fujita, K.; Tagawa, K.; Okazawa, H.; Kubo, K.I.; Nakajima, K. Drebrin-like (Dbnl) controls neuronal migration via regulating N-cadherin expression in the developing cerebral cortex. *J. Neurosci.* **2019**, *39*(4), 678-691.DOI: 10.1523/JNEUROSCI.1634-18.2018

[65] Haenisch, C.; Diekmann, H.; Klinger, M.; Gennarini, G.; Kuwada, J.Y.; Stuermer, C.A. The neuronal growth and regeneration associated Cntn1 (F3/F11/Contactin) gene is duplicated in fish: expression during development and retinal axon regeneration. *Mol. Cell. Neurosci.* ***2005***, *28*(2), 361-374. DOI: 10.1016/j.mcn.2004.04.013

[66] Latremoliere, A.; Cheng, L.; DeLisle, M.; Wu, C.; Chew, S.; Hutchinson, E.B.; Sheridan, A.; Alexandre, C.; Latremoliere, F.; Sheu, S.H.; Golidy, S. Neuronal-specific TUBB3 is not required for normal neuronal function but is essential for timely axon regeneration. *Cell Rep.* **2018**, *24*(7), 1865-1879. DOI: 10.1016/j.celrep.2018.07.029.

[67] Peyrin, J.M.; Deleglise, B.; Saias, L.; Vignes, M.; Gougis, P.; Magnifico, S.; Betuing, S.; Pietri, M.; Caboche, J.; Vanhoutte, P.; Viovy, J.L. Axon diodes for the reconstruction of oriented neuronal networks in microfluidic chambers. *Lab Chip* **2011**, *11*(21), 3663-3673. DOI: 10.1039/C1LC20014C

[68] Kanagasabapathi, T.T.; Massobrio, P.; Barone, R.A.; Tedesco, M.; Martinoia, S.; Wadman, W.J.; Decré, M.M. Functional connectivity and dynamics of cortical–thalamic networks co-cultured in a dual compartment device. *J. Neural Eng.* **2012**, *9*(3), p.036010. DOI: 10.1088/1741-2560/9/3/036010

[69] Berdichevsky, Y.; Staley, K.J.; Yarmush, M.L. Building and manipulating neural pathways with microfluidics. *Lab Chip* **2010**, *10*(8), 999-1004. DOI: 10.1039/B922365G

[70] Serruya, M.D.; Harris, J.P.; Adewole, D.O.; Struzyna, L.A.; Burrell, J.C.; Nemes, A.; Petrov, D.; Kraft, R.H.; Chen, H.I.; Wolf, J.A.; Cullen, D.K. Engineered Axonal Tracts as “Living Electrodes” for Synaptic-Based Modulation of Neural Circuitry. *Adv. Funct. Mater.* **2018**, *28*(12), p.1701183. DOI: 10.1002/adfm.201701183

For Table of Contents Use Only

Manuscript title: Aligned poly-L-Lactic Acid (PLLA) nanofibres induce self-assembly of primary cortical neurons into 3D cell clusters

Authors: Weir, N., Stevens, R., Wagner, S., Miles, A.K., Ball, G.R., Howard, C., Chemmarappally, J.M., McGinnity, T.M., Hargreaves, A.J., Tinsley, C. J.